# Optical self-switching based on a semiconductor-optical-amplifier-assisted Sagnac interferometer

**Morteza Jamali,[1] Vahid Ahmadi,[1,*] and Mohammad Razaghi[2]**

[1]*Department of Electrical and Computer Engineering, Tarbiat Modares University, Tehran, Iran*
[2]*Department of Engineering, University of Kurdistan, Sanandaj, Iran*
**Corresponding author: v_ahmadi@modares.ac.ir*

Received March 12, 2013; revised July 24, 2013; accepted August 7, 2013;
posted August 9, 2013 (Doc. ID 186865); published September 3, 2013

The self-switching mechanism in a Sagnac interferometer is studied numerically. A new structure of a semiconductor-optical-amplifier (SOA)-based Sagnac interferometer self-switch (SISS) is presented. For analyzing the switching characteristics of the structure, an improved finite-difference beam propagation method is utilized to study counterpropagation pulses in the SOA. All intraband nonlinear gain compression effects in the SOA that have not been considered simultaneously in previous Sagnac switches are considered. The effects of structural and input pulse parameters on the SISS operation are analyzed. Simulation results determine the optimum condition for the maximum switching output power. 

*OCIS codes:* (130.4815) Optical switching devices; (120.5790) Sagnac effect; (250.5980) Semiconductor optical amplifiers.
http://dx.doi.org/10.1364/JOSAB.30.002576

## 1. INTRODUCTION

The switching characteristics of semiconductor optical amplifier (SOA) and their other favorable features, such as compactness, low input power, and capability of large-scale optical integration, are the reasons for their extensive application as nonlinear elements for all-optical high-speed switches. Optical nonlinear effects originate from carrier depletion due to the nonlinear behavior of SOAs [1]. SOA-based Sagnac switches have the ability to exhibit a set of logic functions without changing their fundamental design. Self-switching is a technique in which the input signal can be switched to the desired output port by unequally splitting the input light signal into two pulses without using a switching (extra) signal [2], which is also called asymmetric switching [3]. To our knowledge, the SOA-based Sagnac switches presented so far are considered to be symmetric structures with 3 dB couplers, and SOA-based self-switches have been proposed only in Mach–Zehnder interferometer (SOA–MZI)-based structures. SOA–MZI self-switching has been used to perform various tasks, such as all-optical time-domain label recognition [4] and pattern effect compensation [5], and in low-loss optical combiners [6].

In parallel with the use of ultrashort pulses for high-speed switching applications, various new nonlinear effects of SOAs become more important in the subpicosecond regime [7]. The main subpicosecond nonlinear effects are two-photon absorption (TPA), carrier heating (CH), spectral hole burning (SHB), and gain dispersion. In the subpicosecond regime, depending on the shape, width, and power of the input pulse, self-phase modulation (SPM) nonlinearity, which is the main phenomenon for picosecond pulses, will have a considerable effect on pulse shape and spectrum together with the SHB and CH phenomena [8].

We propose here a new Sagnac interferometer self-switch (SISS) structure with a subpicosecond input optical pulse. We predict that the proposed structure has the ability to perform the applications of SOA–MZI self-switches and the logic functions of multiple gate cascades [9]. In this paper, dependency of switching characteristics on structural and input pulse parameters is numerically analyzed. The optimum values of these functional parameters are investigated.

The paper is organized as follows. In Section 2, the structure of our designed self-switch is described and its principle of operation is demonstrated. In Section 3, the theory of interferometric equations that describes the operation of the self-switching scheme is discussed. In Section 4, we introduce the SOA modeling scheme based on modified nonlinear Schrödinger equations (MNLSEs). In Section 5, the results and discussion and the switching characteristics of the proposed structure with its improved and efficient model are presented. Conclusions are given in Section 6.

## 2. SELF-SWITCHING OPERATION PRINCIPLE

The schematic structure of the proposed SOA-based SISS is shown in Fig. 1. The switch consists of two optical loops formed by the joint input and output ports of two independent $2 \times 2$ couplers and an SOA with an InGaAsP/InP material system. The position of the SOA is asymmetric with respect to the center of the two loops. This can be easily adjusted using a commercially available optical delay line (ODL). When an input light enters the loop through one of the input ports (e.g., Port 1; see Fig. 1) of the input coupler, it splits asymmetrically into two counterpropagating pulses ($u$ and $v$). Each coupler induces a $\pi/2$ phase difference between its outputs [10]. The propagation direction of the two pulses is changed by

 

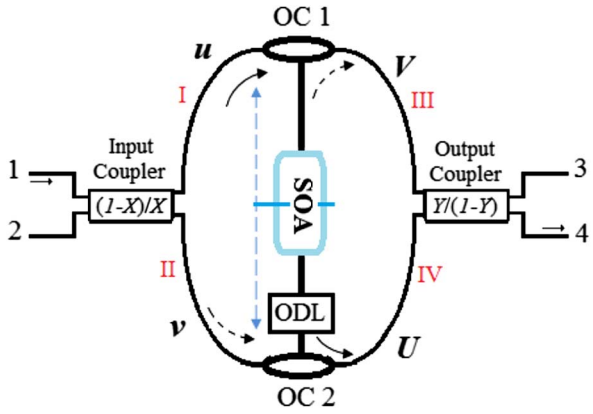


Fig. 1. Schematic structure of the proposed SOA-based SISS. OC, optical circulator; ODL, optical delay line; SOA, semiconductor optical amplifier; $X$ and $Y$, power splitting ratio in the input and output couplers.

two optical circulators (OC1 and OC2). The phase difference induced between the two pulses due to propagation in four waveguides (I to IV) is assumed to be zero. The low-power optical pulse can be injected several picoseconds before the high-power optical pulse or vice versa. These delays cause changes in both the gain and refractive index of the SOA for two counterpropagating pulses and, therefore, the propagating pulses experience different dynamic states. As a result, due to the SOA's nonlinearities, a phase difference occurs between these two pulses. If the phase difference between these pulses reaches an adequate amount ($\pi$) the input pulse in Port 1 will be switched to the switching port (Port 4 in Fig. 1). Note that the proposed SISS is completely different than the SOA-based MZI self-switch structure already presented [5]. In the MZI-based self switch, each data pulse propagates alone in the MZI's arms without any counterpropagation pulse. In the SISS, the data pulses have a counterpropagation geometry in the SOA and, hence, the interactions of data pulses with each other and with the SOA should be considered. As there is no high-intensity control pulse in the self-switch structures, the presented SISS structure is completely different from the cocounter SOA–MZI [11] and typical Sagnac switches [7,9], with different applications.

## 3. THEORY OF PROPOSED SELF-SWITCHING SCHEME

The optical input pulse injected in Port 1 in Fig. 1 is distributed unequally to the $u$ and $v$ pulses. The power splitting ratios in the input and output couplers are $X$ and $1-Y$, respectively. The $u$ and $v$ pulse powers after passing through the input coupler are $P_u = XP_{\text{in}}$ and $P_v = (1-X)P_{\text{in}}$, respectively, where $P_{\text{in}}$ is input power. The low-power optical pulse ($u$ pulse) arrives $\tau_{\text{asym}}$ picoseconds before or after the high-power optical pulse ($v$ pulse). Physically, a negative value means that the $u$ pulse is $\tau_{\text{asym}}$ time units behind the $v$ pulse, while a positive value corresponds to an advance by the same amount of time. As mentioned before, the SOA induces a nonlinear phase shift ($\Delta\varphi$) to optical pulses. When $\Delta\varphi = \pi$, the maximum extinction ratio between switch outputs can be reached. The basic interferometric equations that describe the output pulses with respect to input power at Port 3 and Port 4, respectively, can be written as

$$P_3(t) = \frac{P_{\text{in}}}{2}\{XYG_u(t) + (1-X)(1-Y)G_v(t-\tau_{\text{asym}}) + 2\sqrt{XY(1-X)(1-Y)G_u(t)G_v(t-\tau_{\text{asym}})} \times \cos[\varphi_u(t) - \varphi_v(t-\tau_{\text{asym}})]\} \quad (1)$$

and

$$P_4(t) = \frac{P_{\text{in}}}{2}\{X(1-Y)G_u(t) + (1-X)YG_v(t-\tau_{\text{asym}}) + 2\sqrt{XY(1-X)(1-Y)G_u(t)G_v(t-\tau_{\text{asym}})} \times \cos[\varphi_u(t) - \varphi_v(t-\tau_{\text{asym}})]\}, \quad (2)$$

where $G_u(t)$ and $G_v(t-\tau_{\text{asym}})$ are the SOA gain sensed by the $u$ and $v$ pulses (data pulses) and $\varphi_u(t)$ and $\varphi_v(t-\tau_{\text{asym}})$ are the corresponding phase shifts. These two parameters are related to $\Delta\varphi_{\text{NL}}$ by

$$\Delta\varphi_{\text{NL}} = \varphi_u(t) - \varphi_v(t-\tau_{\text{asym}}) = -\frac{\alpha_N}{2}\ln\left(\frac{G_u(t)}{G_u(t-\tau_{\text{asym}})}\right), \quad (3)$$

where $\alpha_N$ is the linewidth enhancement factor associated with the gain changes due to carrier depletion.

## 4. SOA MODEL

To take into account all nonlinear effects in the SOA for the subpicosecond regime, a set of MNLSEs is solved numerically. The analysis is based on central difference approximation in the time domain and the trapezoidal integration technique for spatial steps [12].

$$\left[\frac{\partial}{\partial z} - \frac{i}{2}\beta_2\frac{\partial^2}{\partial\tau^2} + \frac{\gamma}{2} + \left(\frac{\gamma_{2p}}{2} + ib_2\right)|V(\tau,z)|^2\right]V(\tau,z) = \left\{\frac{1}{2}g_N(\tau)\left[\frac{1}{f(\tau)} + i\alpha_N\right] + \frac{1}{2}\Delta g_T(\tau)(1+i\alpha_T) - i\frac{1}{2}\frac{\partial g(\tau,\omega)}{\partial\omega}\bigg|_{\omega_0}\frac{\partial}{\partial\tau} - \frac{1}{4}\frac{\partial^2 g(\tau,\omega)}{\partial\omega^2}\bigg|_{\omega_0}\frac{\partial^2}{\partial\tau^2}\right\}V(\tau,z), \quad (4)$$

$$g_N(\tau) = g_0\exp\left(-\frac{1}{W_s}\int_{-\infty}^{\tau}e^{-s/\tau_S}|V(s)|^2\mathrm{d}s\right), \quad (5)$$

$$f(\tau) = 1 + \frac{1}{\tau_{\text{SHB}}P_{\text{SHB}}}\int_{-\infty}^{+\infty}U(s)e^{-s/\tau_{\text{SHB}}}|V(\tau-s)|^2\mathrm{d}s, \quad (6)$$

$$\Delta g_T(t) = -h_1\int_{-\infty}^{+\infty}U(s)e^{-s/\tau_{\text{CH}}}(1-e^{-s/\tau_{\text{SHB}}})|V(\tau-s)|^2\mathrm{d}s - h_2\int_{-\infty}^{+\infty}U(s)e^{-s/\tau_{\text{CH}}}(1-e^{-s/\tau_{\text{SHB}}})|V(\tau-s)|^4\mathrm{d}s, \quad (7)$$

and

$$\frac{\partial g(\tau,\omega)}{\partial\omega}\bigg|_{\omega_0} = A_1 + B_1[g_0 - g(\tau,\omega_0)], \quad (8)$$

$$\frac{\partial^2 g(\tau,\omega)}{\partial\omega^2}\bigg|_{\omega_0} = A_2 + B_2[g_0 - g(\tau,\omega_0)], \quad (9)$$

$$g(\tau,\omega_0) = g_N(\tau,\omega_0)/f(\tau) + \Delta g_T(\tau,\omega_0), \quad (10)$$

where $V(\tau,z)$ is the envelope function of an optical pulse and $|V(\tau,z)|^2$ corresponds to the optical power. In Eq. (1), the temporal variation change of the complex envelope function is very slow compared with the cycle of an optical field (slowly varying envelope approximation). $\beta_2$ is the group velocity function, $\gamma$ is linear loss, $\gamma_{2p}$ is the TPA coefficient, $b_2(=\omega_0 n_2/cA)$ is the instantaneous SPM term due to the ultrafast nonlinear refraction, $\omega_0$ is the center angular frequency of input light, $n_2$ is the Kerr effect coefficient, $c$ is the velocity of light in vacuum, $A(=wd/\Gamma)$ is the effective area ($w$ and $d$ are the width and thickness of the active region, and $\Gamma$ is the confinement factor), $g_N(\tau)$ is the saturated gain due to carrier depletion [13,14], $g_0$ is linear gain, $W_s$ is the saturation energy, $\tau_s$ is the carrier lifetime, $f(\tau)$ is the SHB function [15,16], $P_{\mathrm{SHB}}$ is the SHB saturation power, $\tau_{\mathrm{SHB}}$ is the SHB relaxation time, $\alpha_N$ and $\alpha_T$ and are the linewidth enhancement factors associated with the gain change due to carrier depletion and CH, $\Delta g_T(t)$ is the resulting gain change due to CH and TPA, $U(s)$ is the unit step function, $\tau_{\mathrm{CH}}$ is the CH relaxation time, $h_1$ is the contribution of stimulated emission and free carrier absorption to CH gain reduction, and $h_2$ is the contribution of TPA. Finally, $A_1$ and $A_2$ are the slope and curvature of linear gain at $\omega_0$, and $B_1$ and $B_2$ are constants describing changes in these quantities with saturation [17]. The gain spectrum of an SOA can be approximated by the following second-order Taylor expansion in $\omega$:

**Table 1. List of the Parameters Used in Simulation [18]**

| Symbol | Quantity | Value |
|---|---|---|
| $L$ | SOA length | 500 μm |
| $A$ | Effective area | 5 $\mu m^2$ |
| $X(Y=X)$ | Input (output) coupler splitting ratio | 0.3 |
| $E_{\mathrm{in}}$ | Input pulse energy | 1 pJ |
| $\tau_{\mathrm{in}}$ | Input pulse width | 200 fs |
| $f_0$ | Center frequency of the pulse | 193.5 THz |
| $g_0$ | Linear gain | 85 $cm^{-1}$ |
| $\beta_2$ | Group velocity dispersion | 0.045 $ps^2\,cm^{-1}$ |
| $W_s$ | Saturation energy | 10 pJ |
| $\alpha_N$ | Linewidth enhancement factor due to the carrier depletion | 7 |
| $\alpha_T$ | Linewidth enhancement factor due to the CH | 1 |
| $h_1$ | The contribution of stimulated emission and free carrier absorption to CH gain reduction | 0.3 $cm^{-1}\,pJ^{-1}$ |
| $h_2$ | The contribution of two photon absorption | 300 $fs\,cm^{-1}\,pJ^{-2}$ |
| $\tau_s$ | Carrier lifetime | 500 ps |
| $\tau_{\mathrm{CH}}$ | CH relaxation time | 800 fs |
| $\tau_{\mathrm{SHB}}$ | SHB relaxation time | 150 fs |
| $P_{\mathrm{SHB}}$ | SHB saturation power | 11.32 W |
| $\Gamma$ | Linear loss | 15 $cm^{-1}$ |
| $n_2$ | Instantaneous nonlinear Kerr effect coefficient | −0.6 $cm^2\,TW^{-1}$ |
| $\gamma_{2p}$ | Two photon absorption coefficient | 1.6 $cm^{-1}\,TW^{-1}$ |
| $A_1$ | | 0.8 $fs\,\mu m^{-1}$ |
| $B_1$ | Parameters describing second-order Taylor expansion of dynamically gain spectrum | −150 fs |
| $A_2$ | | −150 $fs^2\,\mu m^{-1}$ |
| $B_2$ | | 0 $fs^2$ |

$$g(\tau,\omega) = g(\tau,\omega_0) + \Delta\omega \left.\frac{\partial g(\tau,\omega)}{\partial\omega}\right|_{\omega_0} + \frac{(\Delta\omega)^2}{2}\left.\frac{\partial^2 g(\tau,\omega)}{\partial\omega^2}\right|_{\omega_0}. \quad (11)$$

The coefficients $(\partial g(\tau,\omega))/(\partial\omega)|_{\omega_0}$ and $(\partial^2 g(\tau,\omega)/\partial\omega^2)|_{\omega_0}$ are related to $A_1$, $B_1$, $A_2$, and $B_2$ by Eqs. (8) and (9). We have used the parameters of a bulk SOA (InGaAsP/InP, double heterostructure) with a wavelength of 1.55 μm in the simulation. The parameters are listed in Table 1. We have obtained all the results with a propagation step $\Delta z$ of 500/256 μm.

## 5. RESULTS AND DISCUSSION

Here we consider all nonlinear effects to calculate carrier-dependent nonlinear gain for switching performance. The switch structure is based on an InGaAsP/InP material system and a $\mathrm{sech}^2$ input pulse shape. Listed values in Table 1 are fixed parameters in each figure unless anything else is stated.

Figure 2 shows the SOA dynamic gain response for $u$ and $v$ pulses versus $\tau_{\mathrm{asym}}$. As can be seen, when a $v$ pulse with high power is injected before a low power $u$, the gain that $v$ sees will be saturated and this pulse will be less amplified. However, for the $u$ pulse, because of its lower power, the gain saturation will not occur and higher amplification will occur. The collision of two signal pulses at the input facets of SOA leads to dip shape reduction in the gain profile of $u$ and $v$ pulses at $\tau_{\mathrm{asym}} = -6.3$ ps and $\tau_{\mathrm{asym}} = 6.3$ ps, respectively. By increasing the amount of $\tau_{\mathrm{asym}}$ up to 7 ps, the gain of $u$ increases. For $\tau_{\mathrm{asym}} > 7$ ps, when $v$ is injected, $u$ has already exited from the SOA, so $u$ and $v$ will see the maximum and minimum of gain, respectively. Time variation of the phase difference and its cosine with time offset of the SOA from the midpoint of two Sagnac loops are shown in Fig. 3. This figure shows that, for negative values of $\tau_{\mathrm{asym}}$ ($v$ pulse is injected before $u$ pulse), the differential nonlinear phase shift between two pulses is not large enough for switching ($\Delta\varphi = \pm\pi$). This is due to the fact that when the high-power ($v$) pulse is injected first the gain ratio ($G_u/G_v$) for the pulses will be much lower than the required amount for switching. The increase of positive $\tau_{\mathrm{asym}}$ results in a higher gain ratio and, in turn, the nonlinear phase shift between the two pulses reaches the final value of $\Delta\varphi = -\pi$, which causes the input pulse to be switched to Port 4.

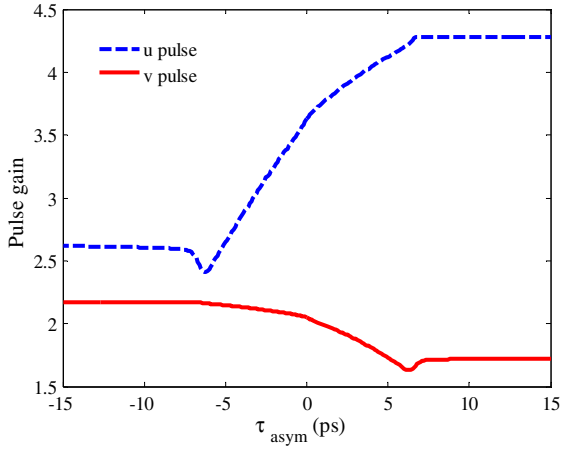


Fig. 2. Dynamic gain response of the SOA for two signal pulses to different offsets of the SOA.

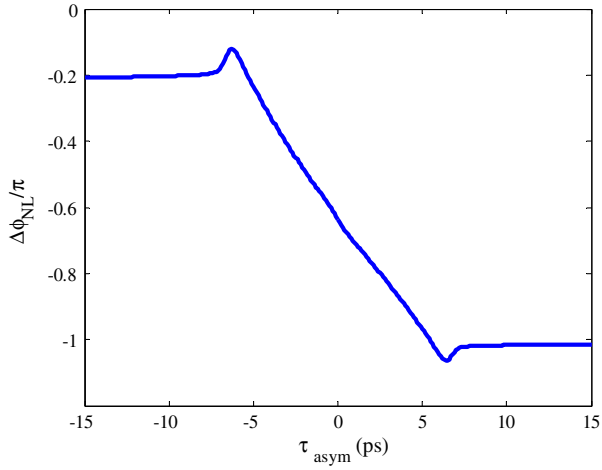


Fig. 3. Variation of phase difference between two signal pulses.

Now we discuss the switching characteristics of the SISS for different operating conditions. Figure 4 illustrates gain ratio versus $\tau_{asym}$ for different values of SOA small signal gain ($g_0$). For $\tau_{asym} < -5$ ps we have higher gain ratio at $g_0 = 60$ cm$^{-1}$ than those of $g_0 = 85$ and 110 cm$^{-1}$. With an increase of $\tau_{asym}$, the gain ratio is increased further for the $g_0 = 110$ cm$^{-1}$ case. By increasing $g_0$, subpicosecond nonlinear effects (especially SHB and CH) are more dominant, producing larger broadening of input pulses. This, in turn, causes a longer collision time between two signal pulses at the input facets of the SOA, leading to a sharper dip/peak shape in the gain ratio profile of the input pulses, which is noticeable for $g_0 = 110$ cm$^{-1}$ in the figure.

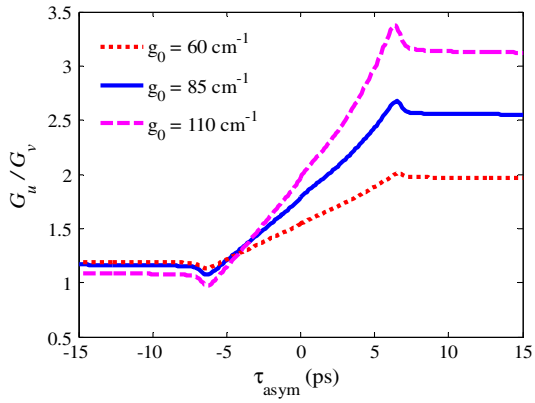


Fig. 4. Gain ratio versus $\tau_{asym}$ for different values of SOA small signal gain ($g_0$).

Figure 5 illustrates normalized output power P4/(P3 + P4) from switching Port 4 versus $\tau_{asym}$ for different values of SOA small signal gain [$g_0$, Fig. 5(a)], and versus $g_0$ for $\tau_{asym} = 10$ ps [Fig. 5(b)]. The inset shows extinction ratio P4/P3 versus $g_0$ for $\tau_{asym} = 10$ ps. In Fig. 5(a), for $\tau_{asym} < -5$ ps, we have higher normalized output power at $g_0 = 60$ cm$^{-1}$ because the gain ratio in this region is larger than those of $g_0 = 85$ and 110 cm$^{-1}$. The dip that appears at around $\tau_{asym} = -6.3$ ps is due to the collision of $u$ and $v$ pulses inside the SOA near the top facet, which leads to reduction in their gain profiles. With an increase of $\tau_{asym}$, the gain ratio is increased further and the normalized output power gets larger for the $g_0 = 110$ cm$^{-1}$ case. Regarding the results shown in Fig. 4, increases in $g_0$ causes the slope of the gain ratio to increase, which, in turn, leads to a higher slope of the normalized output power for $-5$ ps $< \tau_{asym} < 5$ ps in Fig. 5(a). For $g_0 = 110$ cm$^{-1}$, broadening of the input pulses is larger than $g_0 = 85$ cm$^{-1}$ and leads to lower normalized output power for the $g_0 = 110$ cm$^{-1}$ case for $\tau_{asym} > 5$ ps. In Fig. 5(b), variation of normalized output power for different values of small signal gain at $\tau_{asym} = 10$ ps is depicted. According to this figure and its inset, the best operation of the switch is achieved for $g_0 = 85$ cm$^{-1}$. For $g_0 = 85$ cm$^{-1}$, the phase difference between two data pulses reaches $\pi$ and the largest normalized power and extinction ratio (P4/P3) are achieved.

Figure 6 depicts the influence of input pulse energy on the switching characteristics. This is the energy required for achieving a differential phase shift of $\pi$ between the counterpropagating data pulses and, hence, complete constructive interference is reached at the switching port (normalized output power greater than 0.9). In Fig. 6(a) for $E_{in} = 5$ pJ, both data pulses have enough energy to saturate and, hence, the gains that these pulses see will be less than that of $E_{in} = 1$ pJ input energy. In addition, for $E_{in} = 0.2$ pJ input energy the signal pulses have very low energies and gain saturation will not occur, and the gains that the data signal pulses see will be much higher than those of the $E_{in} = 1$ pJ case. For discussion on the

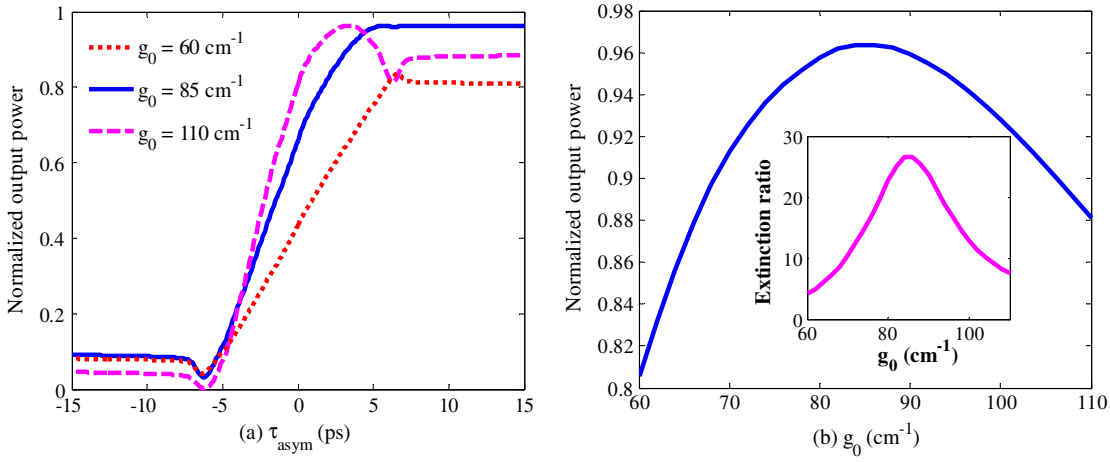


Fig. 5. Normalized output power $P_4/(P_3 + P_4)$ from switched Port 4 versus (a) $\tau_{asym}$ for different values of SOA small signal gain ($g_0$) and (b) $g_0$ for $\tau_{asym} = 10$ ps. The inset shows extinction ratio ($P_4/P_3$) versus $g_0$ for $\tau_{asym} = 10$ ps.

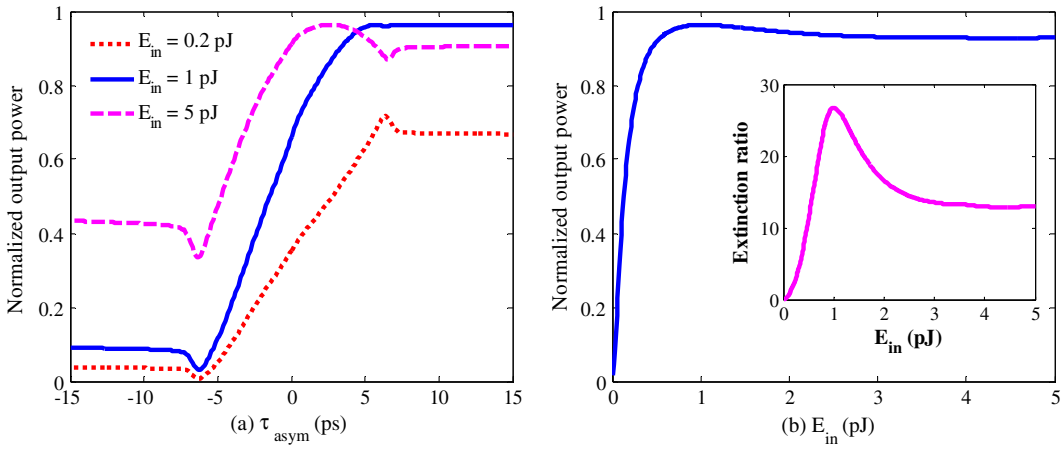


Fig. 6. Normalized output power of switched Port 4 versus (a) $\tau_{asym}$ for different values of input pulse energy and (b) $E_{in}$ for $\tau_{asym} = 10$ ps. The inset shows extinction ratio versus $E_{in}$ for $\tau_{asym} = 10$ ps.

normalized output power we compare the gain ratio for each case. According to Fig. 6(a), for the case of $E_{in} = 5$ pJ, the normalized average power for most values of $\tau_{asym}$ is more than 0.5, which means that the power of the output light in Port 4 is larger than that at Port 3. For $E_{in} = 0.2$ pJ, the normalized average power for most values of $\tau_{asym}$ is less than 0.5, which means that the power of the output light in Port 4 is less than that at Port 3. Figure 6(b) shows that there is threshold input energy to switch the input pulse to Port 4 (normalized output power $\geq$0.9). This threshold energy is approximately 0.5 pJ, at which the phase difference between the two data pulses reaches $\pi$. For higher input energies the phase difference surpasses this a little but will be close to $\pi$, which results in a reduction of the extinction ratio, as clearly shown in the inset of Fig. 6(b). The extinction ratio profile shows that the best input energy is 1 pJ when the other parameters have the values listed in Table 1.

Figure 7 shows the effect of the input pulse width on switch operation. At a fixed pulse energy, the power of the input pulse decreases inversely with the input data pulse width. As shown in Fig. 7(a), for input pulse width ranging from 100 fs to 1 ps, the normalized output powers have relatively the same behavior. For $\tau_{in} = 10$ ps, because of a long pulse width (and lower power with respect to other pulse widths) and negative $\tau_{asym}$, the phase difference will approach the $\pi$ value, which, in turn, leads to higher normalized output power. Figure 7(b) and its inset show the normalized output power and extinction ratio versus $\tau_{in}$ for $\tau_{asym} = 10$ ps, respectively. According to this figure, the normalized output powers are greater than 0.9, i.e., switching occurs for different values of pulse widths. That is, switch operation is approximately independent of pulse width for $\tau_{in} < 1$ ps in single pulse applications. Therefore, 200 fs is a reasonable input pulse width for switch operation. Input pulse power is proportional to input pulse energy divided by input pulse width ($P_{in} \approx E_{in}/\tau_{in}$). According to this relation and the negligible effect or pulse width on SISS operation, we can conclude that peak power equivalent to input pulse energy (shown in Fig. 6) has a significant effect on switch output pulse power.

Figure 8 shows the dependence of the switching characteristics on SOA length ($L$). As this parameter increases, according to Fig. 8(a), the normalized output power starts rising at a smaller value of $\tau_{asym}$. This behavior can be understood by comparing the required time for data pulses to pass through each SOA length. The times required for a data pulse to pass from 700, 500, and 300 μm lengths of SOA with collision to the

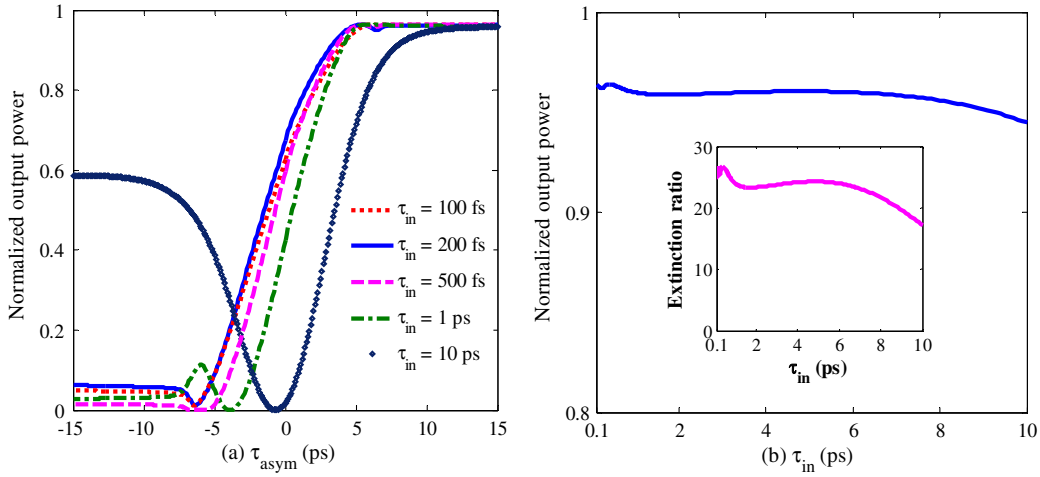


Fig. 7. Normalized output power from switched Port 4 versus (a) $\tau_{asym}$ for different values of input pulse width and (b) $\tau_{in}$ for $\tau_{asym} = 10$ ps. The inset shows extinction ratio versus $\tau_{in}$ for $\tau_{asym} = 10$ ps.

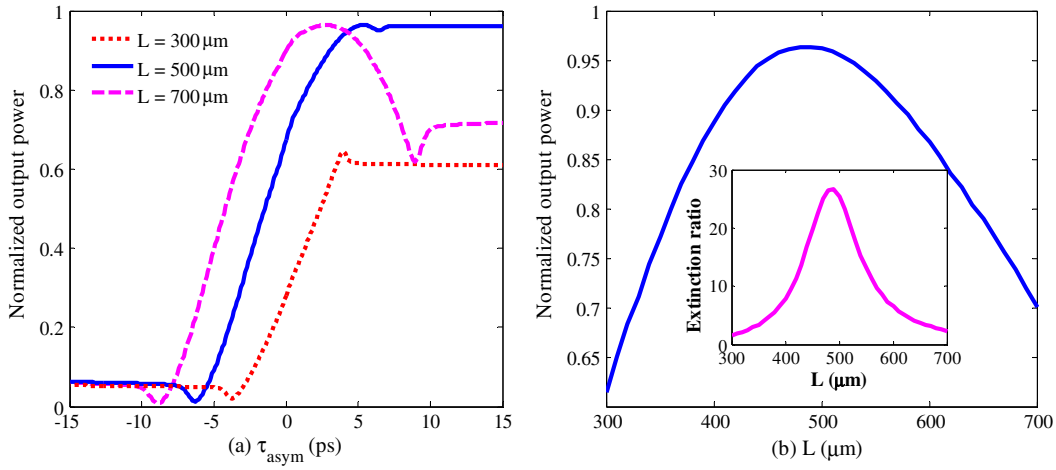


Fig. 8. Normalized output power from switched Port 4 versus (a) $\tau_{asym}$ for different SOA length and (b) $L$ for $\tau_{asym} = 10$ ps. The inset shows extinction ratio versus $L$ for $\tau_{asym} = 10$ ps.

counter pulse are 10, 7, and 4.5 ps, respectively. For example, for $L = 700$ μm, the results show that when $-10$ ps $< \tau_{asym} < 10$ ps, corresponding to the collision condition of the pulses, the normalized output power has some variations. Outside of this interval the normalized output power is fixed because there is no pulse collision. For $L = 300$ μm compared to the two other lengths, the data pulses do not have enough time to reach the required gain ratio and the switching port power. For $L = 700$ μm, due to long $L$, the data pulses gain ratio is more than the required amount and the phase difference will be more than $\pi$, so the power of the switching port decreases. Figure 8(b) illustrates the optimum SOA length to have larger normalized output power and extinction ratio for $\tau_{asym} = 10$ ps. The result reveals that, to have switching operation, the SOA length should be 400 μm $\le L \le$ 570 μm. As depicted in Fig. 8(b), the optimum gain ratio of data pulses occurs at $L = 500$ μm for fixed values of other parameters.

Figure 9 shows the dependence of switching characteristics on the unequal power splitting of the input and output couplers. The input and output couplers' power splitting ratio is the same ($X = Y$). Regarding Fig. 1, for $X = 0.1$, $P_u = 0.1P_{in}$, and $P_v = 0.9P_{in}$. Figure 9(a) depicts the normalized output power of the SISS for the cases of $X = Y = 0.1$, 0.3, and 0.5. The results show that there is no switching operation for the cases of $X = Y = 0.1$ and 0.5. In the case of $X = 0.1$, the phase difference between the data pulses approaches the $\pi$ value for $\tau_{asym} < -4$ ps, and for $\tau_{asym} > -4$ ps it increases up to the $2\pi$ value. The normalized output power is less than 0.9, so switching will not occur. For $X = 0.5$, the two data pulses have equal power. For this case, $X = 0.5$, the required phase difference is induced by the gain ratio. Here the gain ratio is not enough to have a phase difference of $\pi$ for switching. Figure 9(b) and its inset show normalized output power and extinction ratio versus $X$ for $\tau_{asym} = 10$ ps, respectively. As can be observed, the normalized output power has two peaks, at $X = 0.3$ and 0.88. However, switching occurs only for $0.27 < X < 0.37$.

The nonlinearity effect on switch operation is depicted in Fig. 10. The considered parameters are presented in Table 1 for $\tau_{asym} = 10$ ps. This figure compares two cases: all nonlinear effects and only gain saturation effects. For the first, all nonlinear picosecond and subpicosecond effects included in Eqs. (4)–(11) are considered. For the second, only gain

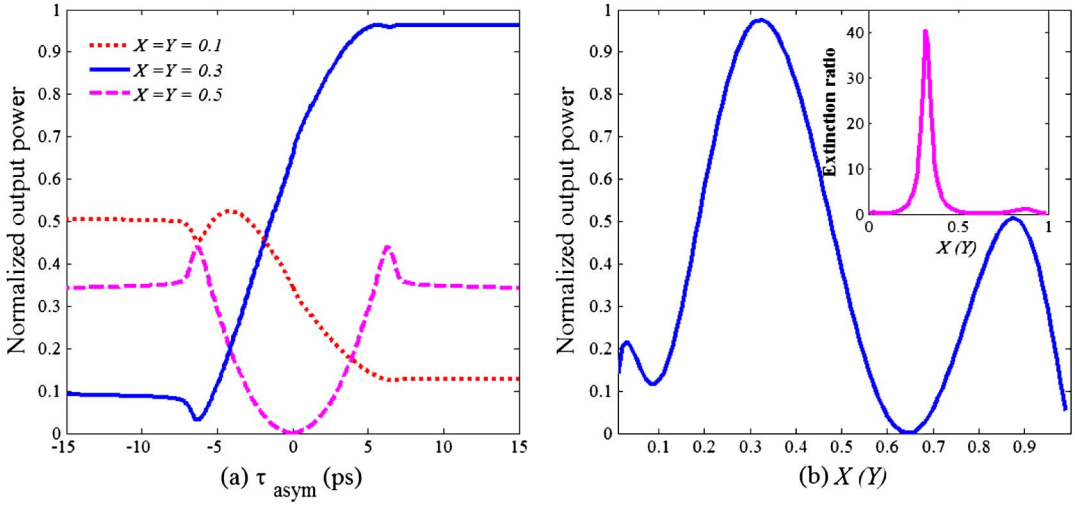


Fig. 9. Normalized output power from switched Port 4 versus (a) $\tau_{asym}$ for different values of couplers splitting coefficient ($X$ and $Y$) and (b) $X(Y)$ for $\tau_{asym} = 10$ ps. The inset shows extinction ratio versus $X(Y)$ for $\tau_{asym} = 10$ ps.

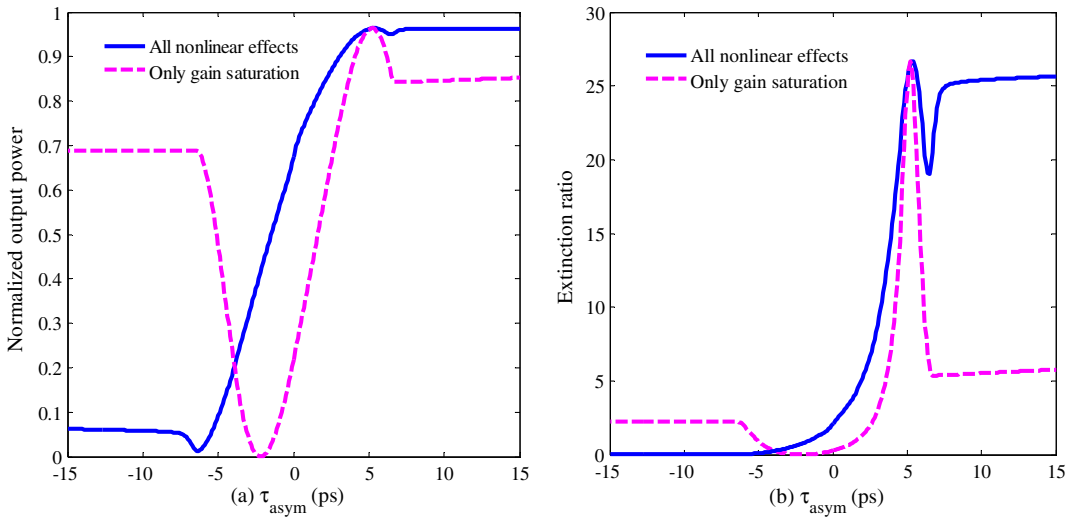


Fig. 10. Effect of subpicosecond nonlinearities on (a) normalized average output power and (b) extinction ratio.

saturation is considered by solving Eq. (4), and other nonlinearities are ignored. As shown in Figs. 10(a) and 10(b), nonlinear subpicosecond effects play an important role in switch operation. For the second case, switching occurs only for 4 ps $< \tau_{asym} <$ 6 ps, and the switch operation is rather similar to the curve of $\tau_{in} = 10$ ps in Fig. 7. This validates our simulation and model because for picosecond pulses (higher than 7 ps) only saturated gain caused by carrier depletion is considered [11]. As shown in Table 1, SHB relaxation time is less than input pulse width ($\tau_{SHB} < \tau_{in}$), which makes it the dominant subpicosecond optical nonlinearity that affects the pulse gain. Hence, SHB induces most of the difference between the results of normalized output power and extinction ratio for both cases, as shown in Fig. 10.

Regarding the results presented in Figs. 5–9, the best values of the design parameters can be extracted as $g_0 = 85$ cm$^{-1}$, $E_{in} = 1$ pJ, $L = 500$ μm, and $X = Y = 0.3$ for the fixed parameters listed in Table 1.

The results for the case of two successive pulses are shown in Fig. 11. The figure shows the normalized output power of switched Port 4 versus input pulse bit rate for the first and second pulses. The fixed parameters are $\tau_{asym} = 10$ ps, $g_0 = 85$ cm$^{-1}$, $\tau_{in} = 200$ fs, $E_{in} = 1$ pJ, $L = 500$ μm, and $X = Y = 0.3$. As shown in the figure, the SOA-based SISS provides appropriate operation for input bit rates of less than 6 Gbits/s. The bit rate should be appropriately chosen corresponding to the $\tau_{asym}$ value.

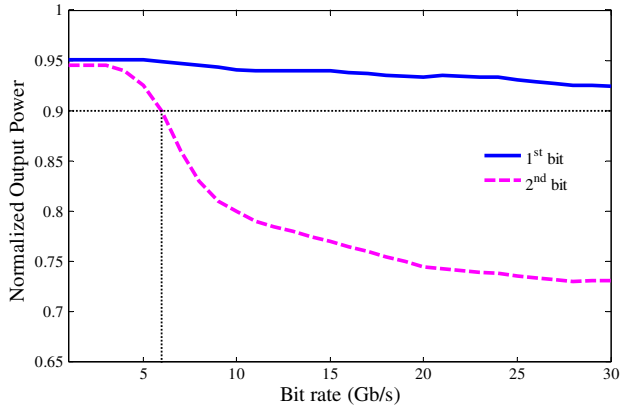


Fig. 11. Normalized output power of switched Port 4 versus input pulse bit rate for the first and second pulses. The fixed parameters are $\tau_{asym} = 10$ ps, $g_0 = 85$ cm$^{-1}$, $\tau_{in} = 200$ fs, $E_{in} = 1$pJ, $L = 500$ μm, and $X = Y = 0.3$.

## 6. CONCLUSION

A new structure for an SOA-based SISS was proposed in this paper. An improved and efficient finite-difference time-dependent beam propagation method was applied to solve the MNLSEs for counterpropagating pulses in an SOA. Simulation studies show the effects of different structural and input pulse parameters on the switching operation of the SISS. For this purpose, the dependencies of normalized output power and extinction ratio on the key performance parameters were investigated. Our simulation results showed the optimum condition for the maximum switching output power. It was shown that couplers with unequal power splitting have significant effect on SISS operation, and input pulse width has small effect on single pulse applications of the SISS.

## REFERENCES

1. M. J. Connelly, *Semiconductor Optical Amplifiers* (Kluwer, 2002).
2. S. Gupta, N. Calabretta, M. Presi, G. Contestabile, A. Wonfor, R. Gangopadhyay, and E. Ciaramella, "Operational equivalence of self-switching in MZI and nonlinear polarization switches based on SOAs," IEEE J. Sel. Top. Quantum Electron. **14**, 779–788 (2008).
3. E. A. Patent, J. J. G. M. Van der Tol, M. L. Nielsen, J. J. M. Binsma, Y. S. Oei, J. Mørk, and M. K. Smit, "Integrated SOA-MZI for pattern-effect-free amplification," Electron. Lett. **41**, 549–551 (2005).
4. J. Kurumida, H. Uenohara, and K. Kobayashi, "All-optical label recognition for time-domain signal using multistage switching scheme based on SOA-MZIs time domain label separation by SOA-MZI self-switching scheme," Electron. Lett. **42**, 1362–1363 (2006).
5. E. A. Patent, J. J. G. M. van der Tol, J. J. M. Binsma, Y. S. Oei, E. A. J. M. Bente, and M. K. Smit, "Self-switching in Mach–Zehnder interferometers with SOA phase shifters," IEEE Photon. Technol. Lett. **17**, 2301–2303 (2005).
6. J. J. G. M. van der Tol, H. de Waardt, and Y. Liu, "A Mach–Zehnder-interferometer-based low-loss combiner," IEEE Photon. Technol. Lett. **13**, 1197–1199 (2001).

7. H. J. S. Dorren, G. D. Khoe, and D. Lenstra, "All-optical switching of an ultrashort pulse using a semiconductor optical amplifier in a Sagnac-interferometric arrangement," Opt. Commun. **205**, 247–252 (2002).
8. M. Razaghi, V. Ahmadi, and M. J. Connelly, "Femtosecond pulse shaping using counter-propagating pulses in a semiconductor optical amplifier," Opt. Quantum Electron. **41**, 513–523 (2009).
9. T. Chattopadhyay and J. N. Roy, "Semiconductor optical amplifier (SOA)-assisted Sagnac switch for designing of all-optical tri-state logic gates," Optik **122**, 1073–1078 (2011).
10. L. B. Soldano and E. C. Penmngs, "Optical multi-mode interference devices based on self-imaging principles and applications," J. Lightwave Technol. **13**, 615–627 (1995).
11. K. I. Kang, T. G. Chang, I. Glesk, and P. R. Prucnal, "Comparison of Sagnac and Mach–Zehnder ultrafast all-optical interferometric switches based on a semiconductor resonant optical nonlinearity," Appl. Opt. **35**, 417–426 (1996).
12. M. Razaghi, V. Ahmadi, and M. J. Connelly, "Comprehensive finite-difference time dependent beam propagation model of counter propagation picosecond pulses in a semiconductor optical amplifier," J. Lightwave Technol. **27**, 3162–3174 (2009).
13. P. Borri, S. Scaffetti, J. Mørk, W. Langbein, J. M. Hvam, A. Mecozzi, and F. Martelli, "Measurement and calculation of the critical pulsewidth for gain saturation in semiconductor optical amplifiers," Opt. Commun. **164**, 51–55 (1999).
14. A. Dienes, J. P. Heritage, C. Jasti, and M. Y. Hong, "Femtosecond optical pulse amplification in saturated media," J. Opt. Soc. Am. B **13**, 725–734 (1996).
15. R. S. Grant and W. Sibbet, "Observations of ultrafast nonlinear refraction in an InGaAsP optical amplifier," Appl. Phys. Lett. **58**, 1119–1121 (1991).
16. A. Mecozzi and J. Mørk, "Saturation induced by picosecond pulses in semiconductor optical amplifiers," J. Opt. Soc. Am. B **14**, 761–770 (1997).
17. M. Y. Hong, Y. H. Chang, A. Dienes, J. P. Heritage, and P. J. Delfyett, "Subpicosecond pulse amplification in semiconductor laser amplifiers: theory and experiment," IEEE J. Quantum Electron. **30**, 1122–1131 (1994).
18. Y. H. Kao, I. V. Goltser, M. Jiang, M. N. Islam, and G. Raybon, "Gain dispersion induced subpicosecond pulse breakup in a fiber and semiconductor laser amplifier combined system," Appl. Phys. Lett. **69**, 4221–4223 (1996).